An Anisotropic Gaussian Filtering Model for Image De-Hazing

HUI FU[ID], **WEIRONG LIU, HUI CHEN, AND ZHIWEN WANG**
College of Electrical and Information Engineering, Lanzhou University of Technology, Lanzhou 730050, China
Corresponding author: Hui Fu (1285110730@qq.com)

ABSTRACT This paper proposes a de-hazing algorithm on the basis of the anisotropic Gaussian filtering method to overcome some essential limitations of the DCP-based (the dark channel prior, DCP) methods, such as halo artifacts and over-saturation problems. In this method, the approximate range of the global atmospheric light A is obtained by using the spatial LOG edge detection method, and the accurate A is acquired by combing binary algorithm. And an anisotropic Gaussian filtering method is adopted to optimize the transmission, which can smooth the rough transmission map, improve the clarity of image details and inhibit halo artifact and over-saturation effect. With the accurate A and optimized transmission, the de-hazing results can be acquired on the basis of the atmospheric scattering model. The processing effect is verified by our own fog image data set constructed in real life or downloaded from the Internet. The visual effect of our method is more natural in brightness, contrast and detail recovery. Besides, the indicators SSIM, PSNR, *Lum*, *Con*, *Inf*, *e* and *r* are relatively high, and indicators MSE and ε are relatively low. Therefore, subjective and objective experimental results demonstrate that our method outperforms four state-of-the-art methods in terms of visual sense definition, robustness and time efficiency.

INDEX TERMS De-hazing, anisotropic Gaussian filtering, clarity, transmission, edge detection.

I. INTRODUCTION

With the deterioration of air pollution, the existence of fog weather has become very frequent and obvious. Generally speaking, fog is produced by scattering of particles such as suspended dust or droplet in the air. This is mainly due to photons being absorbed from the surface and reflected back before being recognized by the optical system. Fog weather conditions both dramatically reduce the visual effect and lead to the reduction of image quality taken by camera sensor, which makes image defogging more and more significant. Under fog weather condition, the visibility of human eyes is obviously reduced, causing many obstacles to outdoor activities and traffic. Currently, many computer vision technologies are required to work in perfect weather condition and high definition environments. Whereas the visibility of objects in an image only relies on the pixel radiance of the scene. In theory, intelligent vehicles, fire monitoring and other image vision applications can only work if the input

image is fog-free. Therefore, contaminated images can bring about serious damage. Hence the study of image defogging is of great value.

In recent years, although single image defogging is an ill-conditioning problem, great progress has been made. In general, image defogging approaches can be roughly classified as two kinds, physics-based defogging algorithms and enhancement-based defogging algorithms. Physics-based defogging algorithms can be divided into two types. The first kinds of methods require multiple images or depth information. For instance, Berman [1] introduced a physical binary scattering model derived from the RGB colour space. By detecting the structural data of foggy scene, fog-free images can be recovered from multiple weather images. Nevertheless, the physical-binary scattering model dose not guarantee better results when dealing with the fog regions similar to the sky. Schechner [2] observed partial polarization of light scattered by atmospheric particles. In response to this phenomenon, they came up with a fast defogging algorithm that captures two images from different angles through a polarizer. Nevertheless, this approach does not apply to all

The associate editor coordinating the review of this manuscript and approving it for publication was Gangyi Jiang.

practical physical models. The second kinds of methods, which require only one image to remove fog, have achieved notable results in recent years. With less prior information of a single fog image, this kind of methods are more challenging. In McLeod's method [3], the radiation function is modeled using gravity distribution, but a large amount of statistical information is needed to assume its independence and restore these functions. He [4] introduced dark channel prior theory (DCP) through multiple observation and combined with soft matting algorithm to restore fog images. However, this method consumes a lot of running time when dealing with the large Laplace matrix. He further combined guided filter [5] with DCP algorithm to process fog images. However, this method performs unsatisfactorily when the color of image scene is close to the atmospheric light. What's more, a variety of DCP-based algorithms [6]–[12] have been proposed. Golts [10] used the approximation of the minimum ellipsoid rather than the assumed minimum. This assumption may also be inaccurate for pixels that associated with bright objects. Wang [11] optimized the atmospheric light by basing on variogram and selected an image area for transmittance estimation. The deblocking operation adopted in this method can remove the noise that may appear after the process of dehazing. With the same idea of removing noise after dehazing processes, the clustering and hidden Markov theory are used to realize the preclassification in Khmag's method [12]. On the basis of Fattal's method [13], Ming [14] applied mathematical models to describe the surface shadow of objects and scene albedo to achieve image defogging. Although this method is physically reliable, it needs to be further refined by using the color-line algorithm. Based on Tarel's method [15], Afridi [16] brought about variables for restoring visibility from a single image under the assumption that depth conversion and spatial change are smooth. This is a logical assumption, but not robust enough to estimate transmittance.

A lot of enhancement-based defogging algorithms are also researched by many scientists, for example, retinex-based algorithms [17]–[20], wavelet-based algorithms [21]–[24], etc. Hu [17] enhanced the fog image with enlarging the local contrast. This method performs better in thick fog regions, whereas the effect is too saturated to avoid halo artifacts. Kasauka [18] employs a multi-scale retinex method to enhance the visibility of different objects in depth scenes. However, the defogging effect will be unsatisfactory when the fog field is not uniform. In Kim's method [22], the overall contrast and brightness of defogging results are good, and achieve a pleasant effect. Nevertheless, this method is difficult to adapt to various foggy scenes.

In short, The physics-based defogging algorithms obtain the fog-free image by analyzing the defogging process, establishing the atmospheric scattering model and inverting the defogging process. However, the atmospheric scattering model is an ill-posed system, which is composed of three functions and at least four unknown parameters per pixel, so it cannot be dealt with directly. The purpose of enhancement-based defogging methods are to compensate the contrast and
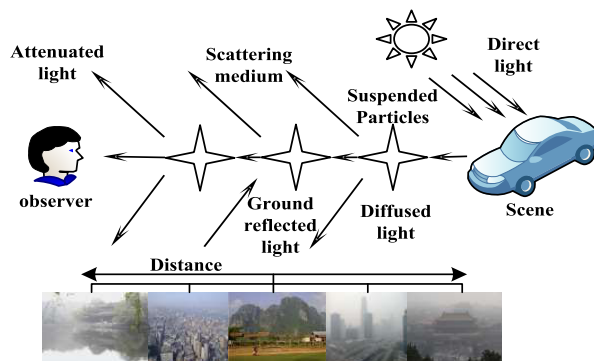

FIGURE 1. Atmospheric scattering model.

color of the degraded image, but at the expense of the depth information of the scene. What's more, these approaches fail to take into account the formation principle of fog image and the mechanism of image degradation.

On the basis of the above analysis, we brought up a novel defogging method in light of accurate estimation of atmospheric light and transmittance in atmospheric scattering physical model.

II. BACKGROUND THEORY
A. ATMOSPHERIC SCATTERING MODEL

Under the fog weather condition, the attenuation and scattering effects of suspended particles on the atmosphere make the overall contrast and color of captured images decrease and fade, respectively. And the above image degradation phenomenon can be represented by Fig.1. In order to simulate and model this phenomenon, Narasimhan [25] deduced the atmospheric scattering model, which has been widely adopted in the field of computer graph and image vision. The atmospheric scattering model can be mathematically expressed as Eq.(1).

$$H(x, y) = R(x, y)t(x, y) + A(1 - t(x, y)) \qquad (1)$$

In it, (x, y) represents the pixel position, $H(x, y)$ the fog image, i.e., the observed intensity, $R(x, y)$ the fog-free image, i.e., the scene radiance. A means the global atmospheric light, $t(x, y)$ the transmission. The term $R(x, y)t(x, y)$ denotes the attenuated light, which is used to describe the remaining part of the scene radiance without decay, and another term $A(1-t(x, y))$ refers to scattered light, which can lead to color shift of image scene. The purpose of image defogging is to recover the fog-free image from the fog image, so it is necessary to estimate the global atmospheric light A and the transmission $t(x, y)$.

In the field of computer vision systems, the transmission can be represented as Eq.(2).

$$t(x, y) = e^{-\beta d(x, y)} \qquad (2)$$

Here, $d(x, y)$ denotes the distance within the target and the observer, β the coefficient of scattering. Owing to the fact that the value of $t(x, y)$, $(0 < t(x, y) \leq 1)$ is independent of the

wavelength, so transmissions of three RGB color channels are the same.

B. THEORY OF DARK CHANNEL PRIOR

After extensive experimental observations, He [5] proposed the DCP theory, that is, the pixel intensity of at least one color channel in the non-sky region of most outdoor fog-free images is close to zero. The dark channel $R^{\mathrm{dark}}(x, y)$ of a fog-free image $R(x, y)$ can be expressed as Eq.(3).

$$R^{dark}(x, y) = \min_{z \in \Omega(x,y)} [\min_{C \in [r,g,b]} R^C(x, y)] \quad (3)$$

Here, $R^C(x, y)$ denotes the RGB channels of $R(x, y)$, $\Omega(x, y)$ a local block centered at (x, y). Therefore, on the basis of dark channel prior, $R^{\mathrm{dark}}(x, y)$ of a fog-free image is close to zero, as shown in Eq.(4).

$$R^{dark}(x, y) \rightarrow 0 \quad (4)$$

Since the global atmospheric light A is a constant, Eq.(5) can be derived from Eq.(1).

$$\frac{H^C(x, y)}{A^C} = \frac{R^C(x, y)t(x, y)}{A^C} + 1 - t(x, y) \quad (5)$$

In it, the superscript $c \in \{r, g, b\}$ means color channels. Supposing that the transmission $t(x, y)$ in a local block is a constant, Eq(5) can be further deduced as Eq.(6).

$$\min_{z \in \Omega(x,y)} (\min_{C \in [r,g,b]} \frac{H^C(x, y)}{A^C})$$
$$= t(x, y) \min_{z \in \Omega(x,y)} (\min_{C \in [r,g,b]} \frac{R^C(x, y)}{A^C}) + 1 - t(x, y) \quad (6)$$

Here, $\min\limits_{z \in \Omega(x,y)} (\min\limits_{C \in [r,g,b]} \frac{H^C(x,y)}{A^C})$ can be considered as the dark channel of the input fog image. Combining formula (4) and formula(6), formula (7) can be obtained.

$$t(x, y) = 1 - \min_{z \in \Omega(x,y)} (\min_{C \in [r,g,b]} \frac{R^C(x, y)}{A^C}) \quad (7)$$

Therefore, the estimation of transmission can be directly obtained from fog images. In order to make the defogging result natural and maintain a good sense of scene depth, the constant w is introduced and set to 0.95, as can be seen in Eq.(8).

$$t(x, y) = 1 - w \cdot \min_{z \in \Omega(x,y)} (\min_{C \in [r,g,b]} \frac{R^C(x, y)}{A^C}) \quad (8)$$

III. ESTIMATION OF A

The global atmospheric light A plays an crucial part in the restoration of fog images and affects the global illumination and the colour of fog-free images. Inaccurate estimation of A will result in poor defogging performance. In Tan's method [26], the maximum value of fog image pixels is regarded as A, whereas the maximum brightness component may belong to the highlighted target area. He [5] used the average pixel value of the first 0.1% of the dark channel as A. This method has strong robustness, while it may result in high A value of

each color channel, thus leading to color deviation. In this paper, the approximate range of A is obtained by using the spatial LOG edge detection method, and the accurate A is acquired by combing binary algorithm.

A. POSITION THE SKY REGION WITH THE SPATIAL LOG EDGE DETECTION METHOD

In this paper, the spatial LOG operator is firstly selected to complete the edge detection of fog image $H(x, y)$. Then 15×15 pixel blocks are searched on both sides of the edge to get the pixel gray value. According to the global atmospheric light A characterized with large value in an image, the location of the sky region can be roughly determined.

LOG method is based on the mathematical model of Gaussian algorithm, as shown in Eq.(9).

$$G(r, \delta) = \frac{1}{2\pi \delta^2} \exp(-\frac{1}{2\delta^2} r^2) \quad (9)$$

In it, $r = \sqrt{x^2 + y^2}$, (x, y) indicates the coordinate of a pixel in an image, δ the scale parameter. Set the initial image as $k(x, y)$, $g(x, y)$ is the result of filtering after convolution operation, as shown below:

$$g(x, y) = G(r, \sigma) * k(x, y) \quad (10)$$

The Laplace operator [27] is selected to perform the derivative operation on the smoothed image, can be described by Eq.(11).

$$\nabla^2 g(x, y) = \nabla^2(G(r, \sigma) * k(x, y)) = (\nabla^2 G(r, \sigma)) * k(x, y) \quad (11)$$

In the formula(13), $\nabla^2 G(r, \sigma)$ is the LOG module, which can be replaced by the spatial LOG operator template, as shown in Fig.2.

FIGURE 2. The spatial LOG operator template.

The LOG operator is also an improvement on the Laplace operator, and can judge the edge by getting the zero position of the second derivative. The traditional Laplace operator is very sensitive to the image noise at the edge. However, the introduction of two-dimensional Gaussian algorithm to complete the filtering can obtain abundant image details, smooth the image noise, eliminate some small isolated points and the junction blocks to a certain extent. LOG algorithm can not only suppress image noises, but also obtain better edge detection results. The convolution of $H(x, y)$ is performed by the discrete template of the LOG operator, the formula (12) can be defined as below:

$$F_1(x, y) = \nabla^2(G(r, \sigma) * F(x, y)) = (\nabla^2 G(r, \sigma)) * F(x, y)$$
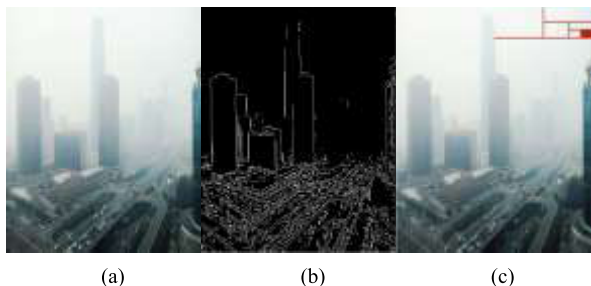$$= \mathbf{LOG}^* F(x, y) \quad (12)$$

FIGURE 3. The spatial LOG edge detection method and binary tree algorithms for obtaining atmospheric light value.(a) Original image (b) LOG edge detection(c) Binary tree estimates atmospheric light value.

The effectiveness after process by LOG method is shown in Fig.3(b).

B. ESTIMATION OF A WITH BINARY TREE ALGORITHM

The sky area detected by the spatial LOG edge detection method is marked as S_1, and then the global atmospheric light A is determined by binary tree method. The principle model of binary tree is shown in Fig.4.
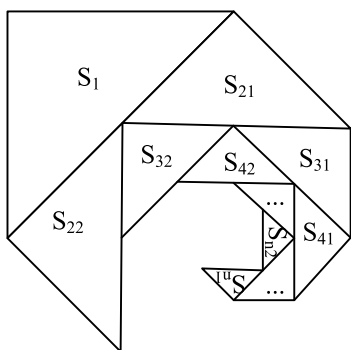

FIGURE 4. The principle model of binary tree.

The specific process is to divide the S_1 region of the original fog image into two identical regions. And calculate and compare the gray mean value of the above two regions. Then set the region with a large gray mean value as S_{21}, complete the next segmentation of S_{21}, and repeat the above steps until the number of pixel points $a[m, n]$ in the region S_{n1} is less than the set threshold value t. The specific image segmentation process of binary-tree method for the global atmospheric light A estimation is shown in Fig.3(c). The equation of pixel points $a[m, n]$ in the region S_{n1} is given by Eq.(13).

$$a[m, n] = \begin{pmatrix} a[0, 0] & a[0, 1] & ... & a[0, n] \\ a[1, 0] & a[1, 1] & ... & a[1, n] \\ ... & ... & ... & ... \\ a[m, 0] & a[m, 1] & ... & a[m, n] \end{pmatrix} \quad (13)$$

Formula (14) shows that each pixel in the $a[m, n]$ matrix is compared with 255, and the difference is set as d. The $a[m, n]$ corresponding to the minimum d value is the global atmospheric light A.

$$d = |255 - a[m, n]| \quad (14)$$

In traditional defogging algorithms, the first 0.1% average pixel value of an fog image is regarded as the global atmospheric light. However, some white or specular reflection objects are often misjudged, and the global atmospheric light A obtained in this way is inevitably subject to large errors. He et al [5] improved the method of estimating A by selecting the brightest 0.1%. However, this method also has its limitations, because the variation of light is nonlinear rather than linear. It is easy to generate "halo effect" after linear processing by He's method. Moreover, the selection of block size has a significant impact on the global atmospheric light, if the selected block is too large, the image details will be weakened; and if the selected block is too small, the image smoothness will be reduced. In this paper, the spatial LOG operator is firstly adopted to locate the global atmospheric light region, and the obtained region is roughly the sky region. Then the global atmospheric light A can be estimated by binary-tree algorithm.

IV. OPTIMIZATION OF TRANSMISSION

Combined with the global atmospheric light A estimated above and substituted into the mathematical model given by Eq.(8), the rough estimation of $t(x, y)$ can be realized. Since the rough transmission $t(x, y)$ changes rapidly with the depth of field and especially at the edge, the edge part of the defogging image is prone to halo effect. In this paper, an anisotropic Gaussian filtering method is adopted to optimize the transmission, which can improve the clarity of image details and inhibit halo artifact and oversaturation effect.

A. THE MATHEMATICAL MODEL OF ANISOTROPIC GAUSSIAN FILTERING METHOD

The traditional Gaussian filter model [28] takes the origin as the core and projects the x and y dimensions, and the projection of the model is a circle. The traditional Gaussian filter model can be expressed as Eq.(15).

$$G(x, y, \delta) = \frac{1}{2\pi \delta^2} \exp(-\frac{1}{2}(\frac{x^2 + y^2}{\delta^2})) \quad (15)$$

In it, δ stands for the scale parameter, θ the direction. The mathematical model of the anisotropic Gaussian filtering can be obtained by setting the proportion of difference between x and y. Its projection forms an ellipse on the two-dimensional plane of the coordinate system, which can be described by formula (16).

$$G(x, y, \delta_x, \delta_y) = \frac{1}{2\pi \delta_x \delta_y} \exp(-\frac{1}{2}(\frac{x^2}{\delta_x^2} + \frac{y^2}{\delta_y^2})) \quad (16)$$

Fig.5(c) shows the image result of converting the image from time domain to frequency domain by rotating the ellipse in Fig.5(b) clockwise along the x-axis and y-axis. And the coordinate transformation model is given by Eq.(17).

$$\begin{bmatrix} u \\ v \end{bmatrix} = \begin{bmatrix} \cos\theta & \sin\theta \\ -\sin\theta & \cos\theta \end{bmatrix} \begin{bmatrix} x \\ y \end{bmatrix} \quad (17)$$
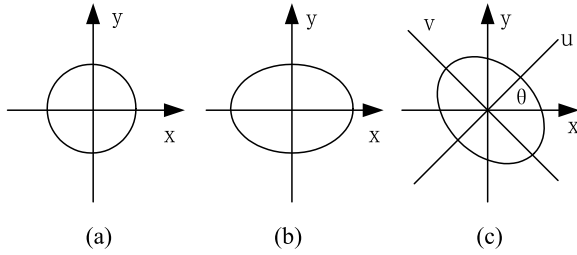
FIGURE 5. Anisotropic Gauss filter model. (a) Gauss filter (b) Anisotropic Gauss filter (c) Anisotropic Gauss filter in frequency domain.

Substitute formula (17) into formula (16) to obtain the frequency domain model of the anisotropic Gaussian filtering, as shown in Eq.(18).

$$G(x, y, \delta_x, \delta_y)$$
$$= \frac{1}{2\pi \delta_x \delta_y} \exp\{-\frac{1}{2}$$
$$\left[\frac{(x\cos\theta + y\sin\theta)^2}{\delta_u^2} + \frac{(-x\sin\theta + y\cos\theta)^2}{\delta_v^2}\right]\} \quad (18)$$

For each part of the image, if the anisotropic Gaussian filtering method is to set a fixed scale parameter δ and a fixed direction parameter θ, that is, the edge and the short axis are consistent with each other, this will lead to the problem that the blur of the image tends to reach the maximum state. While in this paper, the anisotropic Gaussian filtering method can adjust the scale parameter δ and the direction parameter θ according to the image characteristics. The anisotropic Gauss filter model is shown in Fig.5.

B. OPTIMIZATION OF TRANSMISSION BY THE ANISOTROPIC GAUSSIAN FILTERING

The anisotropic Gaussian filtering method can preserve edges and corners of the image, so it has good adaptability and robustness. In this paper, the anisotropic Gaussian filtering method is used to optimize the transmission, which can both smooth the transmission map and save the edge details effectively. The u-axis scale $\delta_u(x, y)$ in Fig.4(c) can be determined by Eq.(19).

$$\delta_u^2(x, y) = 1/t_g(x, y) \quad (19)$$

where, $t_g(x, y)$ is the grayscale value of $t(x, y)$, which is compressed between 0 and 1.

In the smooth area, the proportion of v-axis and u-axis is close to 1, while in the marginal area, the proportion of v-axis and u-axis is close to 0. Therefore, determining the image smoothness is the key to obtain the ratio between the v-axis and u-axis. The gray variance value given by Eq.(20) can represent the smoothness of the transmission.

$$DC = 1/MN \sum_{i=1}^{M} \sum_{j=1}^{N} (t_g(i, j) - \bar{t}_g(i, j))^2 \quad (20)$$

In it, DC denotes the variance within a small region, MN the area of a small image region, $\bar{t}_g(i, j)$ the average gray-value of

a small image region. The ratio R of v-axis and u-axis can be obtained by formula (21).

$$R = K + DC \quad (21)$$

In Eq.(21), assuming that K is the scale parameter, then the scale δ_v of v-axis can be expressed as Eq.(22).

$$\delta_v = R \bullet \delta_u \quad (22)$$

The anisotropic Gaussian filtering method needs to determine the angle θ and the proportion K. Among them, K is the empirical value, and the vertical angle $\theta^\perp$ of the angle θ can be obtained by using the transformation model. The mathematical process of transformation model is described as Eq.(23)-Eq.(25). Take the partial derivatives of the Gaussian function in the x and y directions, and convolve with transmission. Then the vertical angle $\theta^\perp$ of a pixel (x, y) can be obtained.

$$E_x = \frac{\partial G(x, y, \delta)}{\partial x} * t_g(x, y) \quad (23)$$

$$E_y = \frac{\partial G(x, y, \delta)}{\partial y} * t_g(x, y) \quad (24)$$

$$\theta^\perp(x, y) = arctg\left[E_y(x, y)/E_x(x, y)\right] \quad (25)$$

The mathematical relationship between the direction angle θ and the vertical angle $\theta^\perp$ is shown in Formula (26).

$$\theta = \theta^\perp + 90 \quad (26)$$

Substitute formula (26) into formula (18), and formula (27) can be obtained as follows:

$$G_{\theta^\perp}(u, v, \sigma_u, \sigma_v,)$$
$$= \frac{1}{2\pi \sigma_u \sigma_v} \exp\{-\frac{1}{2}$$
$$\left[\frac{(x\cos\theta^\perp + y\sin\theta^\perp)^2}{\sigma_u^2} + \frac{(-x\sin\theta^\perp - y\cos\theta^\perp)^2}{\sigma_v^2}\right]\}$$
$$(27)$$

In Eq.(27), the value of δ_u, δ_v and $\theta^\perp$ can be obtained from the above formula, and the value of K is empirically set as 20. In Fig.6, it can be easily seen that the transmission effect processed by the anisotropic Gaussian filtering method has achieved good results.

C. FOG-FREE IMAGE RESTORATION

With estimation of A and $t(x, y)$, the fog-free image can be recovered from Eq.(28).

$$R(x, y) = \frac{H(x, y) - A}{t(x, y)} + A \quad (28)$$

To avoid the existence of strong noise in the obtained fog-free image when $R(x, y)$ is infinite, the transmission is limited by a lower bound t_0, which is empirically set to 0.1. So Eq.(28) is further expressed as Eq.(29).

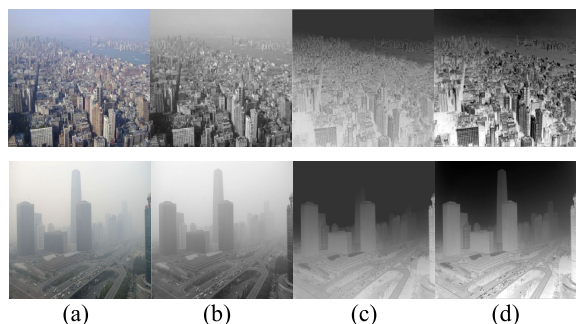$$R(x, y) = \frac{H(x, y) - A}{\max(t(x, y), t_0)} + A \quad (29)$$

FIGURE 6. The transmission effect processed by the adaptive anisotropic Gaussian filter. (a)fog image. (b) greyscale. (c)original transmission. (d)improved transmission.
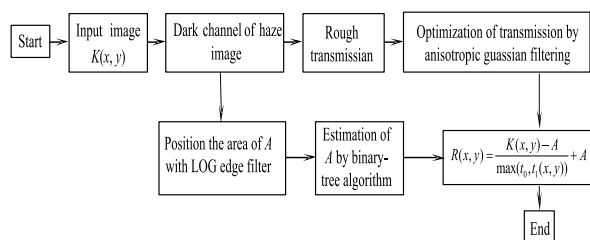

FIGURE 7. The overall framework of our method.

Therefore, it can be seen that the critical point of single image defogging based on atmospheric scattering model is to estimate A and $t(x, y)$. The overall framework of our method is shown as Fig.7.

V. COMPARISON AND ANALYSIS OF EXPERIMENTAL RESULTS

In order to verify that our method can actually and effectively remove fog under various types of scenes, the subjective and objective evaluation methods are used to compare the image quality of four advanced methods (Methods [10], [14], [16], [18]) and the proposed method in fog image processing. Among them, computational complexity, full-reference and no-reference quality assessment indexes are used for the objective evaluation. Besides, each algorithm is analyzed in depth from different angles, and the advantages of our method compared with methods [10], [14], [16], [18] are explained. The experiment platform is built and our algorithm is compiled into a program. The experiment was implemented in the development environment of Matlab 2020a under the 64-bit Windows 10 operating system. And the experimental hardware configuration is Intel Core I7-10750h 3.6GHz and 8GB RAM. The experiment is based on it's own fog image data set, including 896 images captured in real life or downloaded from the Internet, as well as synthetic haze images created, covering a variety of images captured from various shooting angles.

A. SUBJECTIVE EVALUATION

All kinds of fog images were selected for the experiment, including test images of distant and close scenes such as

FIGURE 8. de-hazing effect of our method and other comparing algorithms(a) Original foggy day image. (b) Method [10].(c) Method [14]. (d) Method [16]. (e) Method [18]. (f) our method.

FIGURE 9. de-hazing effect of our method and other comparing algorithms(a) Original foggy day image. (b) Method [10].(c) Method [14]. (d) Method [16]. (e) Method [18]. (f) our method.

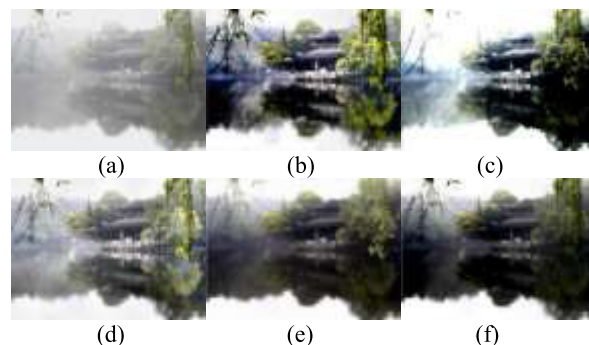**FIGURE 10.** de-hazing effect of our method and other comparing algorithms(a) Original foggy day image. (b) Method [10].(c) Method [14]. (d) Method [16]. (e) Method [18]. (f) our method.
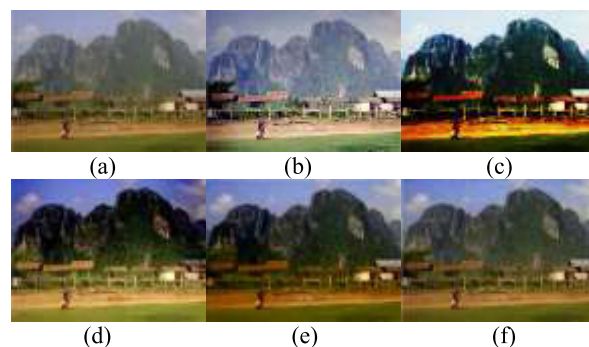
pavilion, plateau grassland and palace buildings, etc. The resolution of Fig.8, Fig.9 and Fig.10 are 360*480, 500*600 and 880*1060, respectively. A comparative analysis was made among the subjective defogging results obtained by methods [10], [14], [16], [18] and our method.

The scene shown in Fig.8(a) is the pavilion image with large sky area. The sky area in Fig.8(b) is dark gray. After being processed by the method [10], the color are artificially deepened to make the effect bright but unnatural. The sky and scenery in Fig.8(c) appear to be heavily whitened, especially in the light-colored areas of the image. Fig.8(d) shows that the overall effect of the defogging result has a lot of noise,

and the degree of fog removal is poor. In Fig.8(e), the overall restoration effect is good, whereas there are still obvious noise areas in the sky area. As can be seen in Fig.8(f), the process effect of our method is more natural in brightness, contrast and detail recovery.

Fig.9 (a) shows a perspective of the plateau grassland. The overall effect of Fig.9 (b) exists a deep color deviation, and the resulting image effect is more similar to a print. This is because the method [10] only artificially improve the image effect by pulling up the contrast and brightness. The effect of Fig.9(c) is white and exists a lot of image noise, which is caused by the inaccurate estimation of transmittance by this method. The image effect shown in Fig.9(d) has a good recovery effect, while the image details are relatively fuzzy. The image effect of method [18] is dark, and the sky region presents obvious image noise. Fig.9(f) shows the result of our method. The retention of a certain amount of fog in the image makes the brightness and sky area more realistic, so the restoration effect is more natural.

Fig.10 (a) shows the local non-uniform fog image formed by industrial pollution in the sky area. The sky area of Fig.10 (b) is deepened by the dense fog, which makes the whole image appear very unnatural. The sky region of Fig.10(c) is similar to the real scene, but the details of the restored image are blurred. The image effect processed by method [16] is seriously distorted, more like an oil painting. The sky area in Fig.10(e) appears as a pan-blue phenomenon without highlighting the details. Fig.10(f) shows the resultant image obtained by our method, which not only truly restore the image details (such as people), but also have better effects compared with the other methods. This is because our method can obtain accurate atmospheric light A and transmittance close to the natural value.

B. OBJECTIVE EVALUATION

1) FULL-REFERENCE QUALITY ASSESSMENT

The full-reference quality assessment is based on the calculation of the difference between the recovered image and the reference image, and then the image quality analysis is completed from the perspective of statistics. The selected reference image is usually an image with ideal scenes, or an image that is processed well by manually changing parameters or different algorithms. In this paper, the indexes peak signal to noise ration (PSNR) [30], mean square Error (MSE) [29] and structure similarity (SSIM) [30] are adopted to evaluate our method. The indexes PSNR and MSE are on the basis of measuring the gray value difference between the recovered image and the reference image, and then the image quality analysis is completed from the perspective of statistics. For an haze image with resolution of $I*J$, $X(x, y)$ is the grayscale result of the reference image in (x, y), and $Y(x, y)$ the grayscale result of the haze image in (x, y). L represents the peak value, for an 8-bit gray image, $L = 2^8 - 1 = 255$.

The function of MSE is shown as below:

$$MSE = \frac{1}{IJ} \sum_{m=1}^{I} \sum_{n=1}^{J} |X(x, y) - Y(x, y)|^2 \qquad (30)$$

And the equation of PSNR is shown as below:

$$PSNR = 10 \log_{10}(\frac{L^2}{MSE}) \qquad (31)$$

The smaller the difference between the recovered image and the reference image, the smaller the image distortion and the better the de-hazing effect.

The SSIM determines the structural similarity of the obtained image according to the degree of correlation between each pixel of the image. $M(x, y)$ and $N(x, y)$ are the reference image and the haze image, respectively. The mean and standard deviation of $M(x, y)$ and $N(x, y)$, and the covariance of $M(x, y)$ and $N(x, y)$ are expressed as $\omega_{X(x,y)}$, $\omega_{Y(x,y)}$, $\delta_{X(x,y)}$, $\delta_{Y(x,y)}$, $\delta_{X(x,y)Y(x,y)}$, individually. To avoid zero denominators, we set parameters o_1, o_2 and o_3. And the functions of brightness $L(X, Y)$, structure $S(X, Y)$, and contrast $C(X, Y)$ can be given by Eq.(32), Eq.(33) and Eq.(34).

$$L(X, Y) = \frac{2\omega_{M(x,y)}\omega_{N(x,y)} + o_1}{\omega_{M(x,y)}^2 + \omega_{N(x,y)}^2 + o_1} \qquad (32)$$

$$S(x, y) = \frac{\delta_{M(x,y)N(x,y)} + o_2}{\delta_{M(x,y)}\delta_{N(x,y)} + o_2} \qquad (33)$$

$$C(x, y) = \frac{2\delta_{M(x,y)}\delta_{N(x,y)} + o_3}{\delta_{M(x,y)}^2 + \delta_{N(x,y)}^2 + o_3} \qquad (34)$$

The index SSIM can be obtained by combining $L(X, Y)$, $S(X, Y)$ and $C(X, Y)$, as shown in Eq.(35).

$$SSIM(x, y) = [L(x, y)]^\alpha [S(x, y)]^\beta [C(x, y)]^\gamma \qquad (35)$$

The index MSE represents the average difference between the recovered image and the reference image. The smaller the result, the better the recovery effect. The index SSIM represents the scene perception of human visual system (HVS), and can measure the structural approximation according to the correlation of each pixel of the image. The larger the result, the better the ability of structure information preservation. The index PSNR indicates the difference between the recovered image and the reference image. The larger the result, the smaller the distortion of image effect. The average results of full-reference evaluation indexes obtained by methods [10], [14], [16], [18] and our method for 92 images in the fog image data set were calculated. The full-reference quality evaluation results of methods [10], [14], [16], [18] and our method are shown as Tab.1. With more accurate atmospheric light A and transmission $t(x, y)$, the closer to the real effect of the dehazing effect can be obtained. So the full-reference quality assessment of our method is relatively good.

TABLE 1. The full-reference quality evaluation results of methods [10], [14], [16], [18] and our method.

	MSE(10^2)	SSIM	PSNR
Method [10]	11.9865	0.7601	16.9925
Method [14]	12.1082	0.7652	20.5823
Method [16]	12.8692	0.7709	19.0912
Method [18]	10.5839	0.7762	19.8519
Improved method	9.1804	0.7859	21.8692

2) NO-REFERENCE QUALITY ASSESSMENT

The no-reference quality assessment indexes [31], [32] we used in this paper include new visible edge ratio e, mean gradient ratio r, the exposure ratio ε.

$$e = \frac{n_{out} - n_{in}}{n_{in}} \tag{36}$$

$$r = \frac{g_{in}}{g_{out}} \tag{37}$$

$$\varepsilon = \frac{v_b}{S_x \times S_y} \tag{38}$$

where, n_{out} and n_{in} denote the number of visible edges of the haze-free image and the haze image, respectively. g_{out} and g_{in} mean the average gradient of the haze-free image and the haze image, individually. S_x and S_y represent the width and height of the image, respectively. v_b represents the number of overexposed or underexposed pixels in a recovered image.

The index e denotes the complexity of the image hierarchy. The larger e is, the more layer and details are contained in the image. The index r represents the contrast and detail enhancement of the image. The higher the value, the better the contrast and detail enhancement. The indicator ε means the status of overexposure or underexposure in the image, and the smaller the value, the less exposure problems.

Lum refers to the mean pixel brightness of the recovered image. The higher the *Lum*, the better the image effect.

$$Lum = \frac{1}{IJ} \sum_{i=1}^{I} \sum_{j=1}^{J} H(x, y) \tag{39}$$

Information entropy *Inf* represents the average amount of data in an image, which measures the amount of data in an image from the perspective of information theory. The higher the information entropy of the image, the more data the image contains.

$$Inf = -\sum_{l=0}^{L} T(l) \log T(l) \tag{40}$$

where, $T(l)$ is the probability of grayscale l occurring in the processed image. L means the total number of grayscale levels of the recovered image. For an image with 256 grayscale levels, L is 255.

Contrast *Con* can measure the sharpness of an image. The image with good visual effect has a high contrast, while the blurred image has a low contrast. And the index *Con* can be

TABLE 2. The no-reference quality evaluation results of methods [10], [14], [16], [18] and our method.

Index	images	*Lum*	*Con*	*Inf*	*e*	*r*	*ε*
Method [10]	Fig.8(b)	132.6	51.6	7.6518	0.7592	1.6149	0.1129
	Fig.9(b)	88.9	55.2	7.3814	0.5613	1.3694	0.1652
	Fig.10(b)	96.1	41.9	7.1056	0.5031	1.4091	0.1581
Method [14]	Fig.8(c)	**205.8**	32.2	6.4219	0.2292	1.2911	0.2832
	Fig.9(c)	**146.2**	46.8	7.1126	0.5019	1.6008	0.2145
	Fig.10(c)	126.9	41.5	7.3106	**0.6295**	1.5021	0.1693
Method [16]	Fig.8(d)	191.2	30.5	6.2659	0.2015	1.2285	0.3030
	Fig.9(d)	123.8	41.9	7.4259	0.8952	1.7138	0.1256
	Fig.10(d)	142.5	29.8	6.3392	0.3062	1.2692	0.1869
Method [18]	Fig.8(e)	129.6	46.3	7.1826	0.5183	1.5591	0.1291
	Fig.9(e)	78.9	38.5	7.6603	0.7845	1.5846	0.1615
	Fig.10(e)	118.6	41.6	7.1049	0.5691	1.3621	0.1387
Improved method	Fig.8(f)	165.2	**56.8**	7.5216	0.7789	1.6692	**0.0912**
	Fig.9(f)	149.5	**61.9**	7.8115	0.8192	1.7283	**0.0997**
	Fig.10(f)	**152.8**	45.8	7.2915	0.6175	**1.5319**	**0.1153**

defined by Eq.(41).

$$Con = \frac{1}{IJ} \sum_{i=1}^{I} \sum_{j=1}^{J} C(x, y) \tag{41}$$

In Eq.(41), *Con* means the contrast of the $I * J$ image, and $C(x, y)$ the contrast of the adjacent region of pixel point (x, y).

The no-reference quality evaluation results of methods [10], [14], [16], [18] and our method is shown as Tab.2.

3) COMPUTATIONAL COMPLEXITY

The computational complexity is judged by comparing the processing time of each algorithm. In order to test the computational complexity of four advanced algorithms more effectively, each algorithm was run several times in the experiment platform and the average processing time was obtained. The method [10] optimized atmospheric light A and transmittance $t(x, y)$ by making the approximation of the minimum ellipsoid. While the process of optimizing transmittance limits the processing efficiency. The algorithm [14] applies mathematical models to describe the surface shadow of objects and scene albedo to achieve image defogging, which consumes a lot of processing time in modeling. The algorithm [16] brought about variables for restoring visibility from a single image under the assumption that depth conversion and spatial change are smooth. However, as the image scale increases, the processing time of the algorithm also increases. The algorithm [18] uses MSR algorithm to get the light component and reflection component of the image, and then utilizes the Laplace pyramid to process the reflection component to enhance the details of the image. This method can avoid the time loss without calculating model parameters. In this paper, the spatial LOG edge detection method and binary tree algorithm are combined to obtain A, and the anisotropic Gaussian filtering method is used to optimize the transmission. These options can not only obtain good image effect, but also save processing time. From the perspective of algorithm complexity, the time loss of our method is mainly in the process of transmission optimization. Compared with
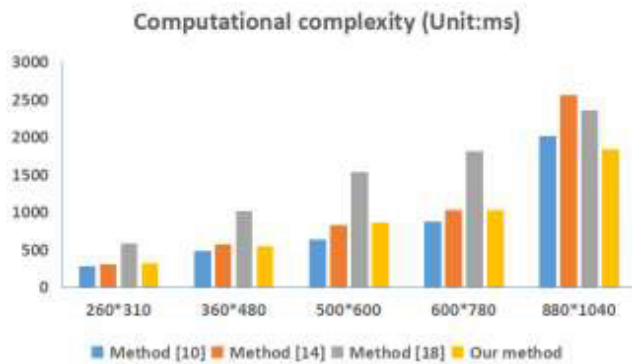
FIGURE 11. Computational complexity.

TABLE 3. Computational complexity. (Unit:ms).

Resolution	260*310	360*480	500*600	600*780	880*1040
Method [10]	275.6	485.1	632.9	872.5	2015.2
Method [14]	312.4	569.2	831.5	1025.1	2561.3
Method [16]	1969.8	5615.8	7319.6	11571.6	15628.3
Method [18]	586.1	1014.2	1539.6	1819.3	2365.2
Our method	316.9	551.3	869.3	1032.4	1835.2

the time domain operation, the addition and multiplication of pixel-level data in frequency domain performed by the anisotropic Gaussian filter method in this paper can better meet the requirements of frequent operation processing and storage. Therefore, the calculation amount of our method is small and the processing speed is fast. As can be seen in Tab.3, the processing time of the algorithm [16] is obviously very long, so Fig.11 only compares the computational complexity of the proposed method with that of methods [10], [14], [18].

VI. SUMMARY

Our method is proposed on the basis of the DCP theory of He's method. In his method, the global atmospheric light A is obtained by calculating the average pixel value of the first 0.1% of the dark channel. This method has strong robustness, while it may result in high A value of each color channel, thus leading to color deviation. And He [5] combined guided filter with DCP algorithm to process transmission. However, his method performs unsatisfactorily because of the inaccurate estimation of transmission. In order to obtain the accurate atmospheric light value and the optimized transmission, the approximate range of A is obtained by using the spatial LOG edge detection method, and the accurate A is acquired by combing binary algorithm. And an anisotropic Gaussian filtering method is adopted to optimize the transmission, which can improve the clarity of image details and inhibit halo artifact and over-saturation effect. Therefore, the key contribution of our method is to use simple and effective methods to accurately estimate global atmospheric light and transmission.

In addition, the main contributions of our approach are listed as below.

Combined with the spatial LOG edge detection method and binary tree algorithm to obtain A, the real-time performance of our method is improved.

The existence of large sky area in haze image scene often has a negative effect on the calculation of the atmospheric light A. While the spatial LOG edge detection method adopted in this paper is especially suitable for processing this kinds of haze images.

The anisotropic Gaussian filtering method can preserve the edges and corners of the image, which has good adaptability and robustness.

In the future work, we will further improve the speed of the algorithm, and extend the static image de-hazing to real-time video de-hazing. In addition to fog images, images captured under other extreme meteorological conditions, such as rain, dust and snow, also need to be further researched.

REFERENCES

[1] D. Berman, T. Treibitz, and S. Avidan, "Single image dehazing using haze-lines," *IEEE Trans. Pattern Anal. Mach. Intell.*, vol. 42, no. 3, pp. 720–734, Mar. 2020.

[2] M. Kaur, D. Singh, V. Kumar, and K. Sun, "Color image dehazing using gradient channel prior and guided l0 filter," *Inf. Sci.*, vol. 521, pp. 326–342, Jun. 2020.

[3] X. Luo, A. Jonathan McLeod, S. E. Pautler, C. M. Schlachta, and T. M. Peters, "Vision-based surgical field defogging," *IEEE Trans. Med. Imag.*, vol. 36, no. 10, pp. 2021–2030, Oct. 2017.

[4] K. He, J. Sun, and X. Tang, "Single image haze removal using dark channel prior," *IEEE Trans. Pattern Anal. Mach. Intell.*, vol. 33, no. 12, pp. 2341–2353, Dec. 2011.

[5] K. He, J. Sun, and X. Tang, "Guided image filtering," *IEEE Trans. Pattern Anal. Mach. Intell.*, vol. 35, no. 6, pp. 1397–1409, Jun. 2013.

[6] W. Wang, F. Chang, T. Ji, and X. Wu, "A fast single-image dehazing method based on a physical model and gray projection," *IEEE Access*, vol. 6, pp. 5641–5653, 2018.

[7] H. Fu, B. Wu, Y. Shao, and H. Zhang, "Scene-awareness based single image dehazing technique via automatic estimation of sky area," *IEEE Access*, vol. 7, pp. 1829–1839, 2019.

[8] W. Lou, Y. Li, G. Yang, C. Chen, H. Yang, and T. Yu, "Integrating haze density features for fast nighttime image dehazing," *IEEE Access*, vol. 8, pp. 113318–113330, 2020.

[9] H. Fu, B. Wu, and Y. Shao, "Multi-feature-based bilinear CNN for single image dehazing," *IEEE Access*, vol. 7, pp. 74316–74326, 2019.

[10] A. Golts, D. Freedman, and M. Elad, "Unsupervised Single Image dehazing Using Dark Channel Prior Loss," *IEEE Trans. Image Process.*, vol. 29, pp. 2692–2701, 2020.

[11] J.-B. Wang, N. He, L.-L. Zhang, and K. Lu, "Single image dehazing with a physical model and dark channel prior," *Neurocomputing*, vol. 149, pp. 718–728, Feb. 2015.

[12] A. Khmag, S. A. R. Al Haddad, R. A. Ramlee, N. Kamarudin, and F. L. Malallah, "Natural image noise removal using nonlocal means and hidden Markov models in transform domain," *Vis. Comput.*, vol. 34, no. 12, pp. 1661–1675, Dec. 2018.

[13] R. Fattal, "Single image de-hazing," *ACM Trans. Graph.*, vol. 27, no. 3, pp. 988–992, Aug. 2008.

[14] M. Ju, C. Ding, Y. J. Guo, and D. Zhang, "IDGCP: Image dehazing based on gamma correction prior," *IEEE Trans. Image Process.*, vol. 29, pp. 3104–3118, May 2020.

[15] J.-P. Tarel and N. Hautiere, "Fast visibility restoration from a single color or gray level image," in *Proc. IEEE 12th Int. Conf. Comput. Vis.*, Sep. 2009, pp. 2201–2208.

[16] I. U. Afridi, T. Bashir, H. A. Khattak, T. M. Khan, and M. Imran, "Degraded image enhancement by image dehazing and directional filter banks using depth image based rendering for future free-view 3D-TV," *PLoS ONE*, vol. 14, no. 5, May 2019, Art. no. e0217246.

[17] H.-M. Hu, H. Zhang, Z. Zhao, B. Li, and J. Zheng, "Adaptive single image dehazing using joint local-global illumination adjustment," *IEEE Trans. Multimedia*, vol. 22, no. 6, pp. 1485–1495, Jun. 2020.

[18] D. Kasauka, K. Sugiyama, H. Tsutsui, H. Okuhata, and Y. Miyanaga, "An architecture for real-time retinex-based image enhancement and haze removal and its FPGA implementation," *IEICE Trans. Fundam. Electron., Commun. Comput. Sci.*, vol. 102, no. 6, pp. 775–782, Jun. 2019.

[19] L. Michela, "Generalized equation for real-world image enhancement by Milano Retinex family," *J. Opt. Soc. Amer. A, Opt. Image Sci.*, vol. 37, no. 5, pp. 849–858, May 2020.

[20] J.-L. Lisani, J.-M. Morel, A.-B. Petro, and C. Sbert, "Analyzing center/surround retinex," *Inf. Sci.*, vol. 512, pp. 741–759, Feb. 2020.

[21] H. Khan, M. Sharif, N. Bibi, M. Usman, S. A. Haider, S. Zainab, J. H. Shah, Y. Bashir, and N. Muhammad, "Localization of radiance transformation for image dehazing in wavelet domain," *Neurocomputing*, vol. 381, pp. 141–151, Mar. 2020.

[22] S. E. Kim, T. H. Park, and I. K. Eom, "Fast single image dehazing using saturation based transmission map estimation," *IEEE Trans. Image Process.*, vol. 29, pp. 1985–1998, May 2020.

[23] U. A. Nnolim, "Single image de-hazing using adaptive dynamic stochastic resonance and wavelet-based fusion," *Optik*, vol. 195, Oct. 2019, Art. no. 163111.

[24] A. Khmag, S. A. R. Al-Haddad, A. R. Ramli, and B. Kalantar, "Single image dehazing using second-generation wavelet transforms and the mean vector L2-norm," *Vis. Comput.*, vol. 34, no. 5, pp. 675–688, May 2018.

[25] S. G. Narasimhan and S. K. Nayar, "Interactive (de) weathering of an image using physical models," in *Proc. IEEE Workshop Color Photometric Methods Comput. Vis.*, Paris, France, Oct. 2003, pp. 1–8.

[26] R. T. Tan, "Visibility in bad weather from a single image," in *Proc. IEEE Conf. Comput. Vis. Pattern Recognit.*, Jun. 2008, pp. 1–8.

[27] J. P. Barbosa, L. O. C. Lara, and C. F. Loeffler, "The domain superposition technique for solving three-dimensional piecewise homogeneous laplace problems," *Int. J. Solids Struct.*, vol. 199, pp. 85–94, Aug. 2020.

[28] S. B. Fazili and M. Ahmad, "Guassian gradient descent model for trust inference in imbalanced data," in *Proc. 2nd Int. Conf. Intell. Comput. Control Syst. (ICICCS)*, Madurai, India, Jun. 2018, pp. 929–934.

[29] D. Sandic-Stankovic, D. Kukolj, and P. Le Callet, "Image quality assessment based on pyramid decomposition and mean squared error," in *Proc. 23rd Telecommun. Forum Telfor (TELFOR)*, Belgrade, Serbia, Nov. 2015, pp. 740–743.

[30] A. Horé and D. Ziou, "Image quality metrics: PSNR vs. SSIM," in *Proc. 20th Int. Conf. Pattern Recognit.*, Istanbul, Turkey, Aug. 2010, pp. 2366–2369.

[31] K. Wang, H. Wang, Y. Li, Y. Hu, and Y. Li, "Quantitative performance evaluation for dehazing algorithms on synthetic outdoor hazy images," *IEEE Access*, vol. 6, pp. 20481–20496, 2018.

[32] H. Fu, B. Wu, Y. Shao, and H. Zhang, "Perception oriented haze image definition restoration by basing on physical optics model," *IEEE Photon. J.*, vol. 10, no. 3, pp. 1–16, Jun. 2018.

WEIRONG LIU is currently a Professor and a Doctoral Supervisor. In July 1999, he joined the Lanzhou University of Technology and engaged in teaching and research work. For many years, he has been devoted to the research of advanced control theory and application of complex systems, image processing, and artificial intelligence. He has been in charge of more than ten national and provincial-level vertical scientific research projects, including the National Natural Science Foundation of China, the Western Part of the National Science and Technology Research Program, and the Key Science and Technology Project of Gansu province. He has also been in charge of more than ten major technology contract projects. He has obtained one first prize of provincial science and technology progress, three third prize of provincial science and technology progress, and many department and bureau awards. Besides, he has published more than 20 academic papers in important academic journals and conferences at home and abroad, and has long served as a review expert of many international journals, conferences, and projects funded by the National Natural Science Foundation of China.

HUI CHEN received the Ph.D. degree from Xi'an Jiaotong University. He is currently a Professor, a Doctoral Supervisor, and a flying Scholar of Gansu province. He is the winner of the young teachers' Achievement Award in colleges and universities in Gansu province, and was selected as the young innovation and entrepreneurship talent in Longyuan. He has published more than 40 papers indexed by SCI and EI in academic journals and conferences at home and abroad as the first author. He is currently a peer review expert of foundation projects of the National Natural Science Foundation of China, and a review expert of doctoral foundation of higher education institutions of the Ministry of Education. He has presided over three national Natural Science Foundation projects, three natural science foundation projects of Gansu province, and one education department project of Gansu province.

HUI FU received the B.E., M.S., and Ph.D. degrees from the School of Information Engineering, Southwest University of Science and Technology, Mianyang, China, in 2014, 2017, and 2020, respectively. She is currently a Teacher with the Lanzhou University of Technology. Her research interests include image processing, deep learning, and computer vision.

ZHIWEN WANG received the B.E. degree from Xi'an Jiaotong University, Xi'an, China, in 1999, and the M.S. and Ph.D. degrees from the Lanzhou University of Technology, Lanzhou, China, in 2004 and 2007, respectively. In 2010, he went to the China University of Mining and Technology for visiting and exchange. In 2013, he entered the Bossy Mobile Station of Control Science and Engineering, Dalian University of Technology. In 2014, he obtained the professorship. And he is a Doctoral Supervisor. His research interests include the industrial control theory and image processing. He has presided over and participated in more than ten national and provincial projects and published more than 30 academic articles.

● ● ●